



OPEN

Inhibiting SARS-CoV-2 infection in vitro by suppressing its receptor, angiotensin-converting enzyme 2, via aryl-hydrocarbon receptor signal

Keiji Tanimoto^{1✉}, Kiichi Hirota², Takahiro Fukazawa³, Yoshiyuki Matsuo², Toshihito Nomura⁴, Nazmul Tanuza⁴, Nobuyuki Hirohashi¹, Hidemasa Bono⁵ & Takemasa Sakaguchi⁴

Since understanding molecular mechanisms of SARS-CoV-2 infection is extremely important for developing effective therapies against COVID-19, we focused on the internalization mechanism of SARS-CoV-2 via ACE2. Although cigarette smoke is generally believed to be harmful to the pathogenesis of COVID-19, cigarette smoke extract (CSE) treatments were surprisingly found to suppress the expression of ACE2 in HepG2 cells. We thus tried to clarify the mechanism of CSE effects on expression of ACE2 in mammalian cells. Because RNA-seq analysis suggested that suppressive effects on ACE2 might be inversely correlated with induction of the genes regulated by aryl hydrocarbon receptor (AHR), the AHR agonists 6-formylindolo(3,2-b)carbazole (FICZ) and omeprazole (OMP) were tested to assess whether those treatments affected ACE2 expression. Both FICZ and OMP clearly suppressed ACE2 expression in a dose-dependent manner along with inducing CYP1A1. Knock-down experiments indicated a reduction of ACE2 by FICZ treatment in an AHR-dependent manner. Finally, treatments of AHR agonists inhibited SARS-CoV-2 infection into Vero E6 cells as determined with immunoblotting analyses detecting SARS-CoV-2 specific nucleocapsid protein. We here demonstrate that treatment with AHR agonists, including FICZ, and OMP, decreases expression of ACE2 via AHR activation, resulting in suppression of SARS-CoV-2 infection in mammalian cells.

Severe acute respiratory syndrome coronavirus 2 (SARS-CoV-2), which was first reported in Wuhan, China in December 2019, is rapidly and continuously spreading all over the world [World Health Organization (WHO)/Coronavirus disease (SARS-CoV-2 induced disease: COVID-19) pandemic]¹. Many epidemiological studies have suggested that smoking habits have serious effects on the pathogenesis of COVID-19²⁻⁵. Expression of the receptor for SARS-CoV-2 infection, angiotensin-converting enzyme 2 (ACE2), was also reported to be higher in smoking mice and humans, suggesting that smokers may be at a higher risk of infection⁶. On the other hand, several reports suggested fewer smokers among patients infected with SARS-CoV-2 or lower numbers of SARS-CoV-2 positive cases among smokers than among non-smokers⁷⁻¹⁰. Therefore, the impact of smoking on SARS-CoV-2 infection is unclear. Cigarette smoke contains a variety of compounds, such as polycyclic aromatic hydrocarbons (PAHs) and nitrosamines, and cellular responses to cigarette smoke exposure are thus diverse^{11,12}. PAHs bind to and activate aryl hydrocarbon receptor (AHR, which is an intracellular receptor type transcription factor), and induce various cellular physiological and pathological responses through the regulation of gene expression^{13,14}. AHR is also activated by a broad variety of exogenous and endogenous small molecular weight

¹Department of Radiation Disaster Medicine, Research Institute for Radiation Biology and Medicine, Hiroshima University, Hiroshima 734-8553, Japan. ²Department of Human Stress Response Science, Institute of Biomedical Science, Kansai Medical University, Hirakata 573-1010, Japan. ³Natural Science Center for Basic Research and Development, Hiroshima University, Hiroshima 734-8553, Japan. ⁴Department of Virology, Graduate School of Biomedical and Health Sciences, Hiroshima University, Hiroshima 734-8553, Japan. ⁵Program of Biomedical Science, Graduate School of Integrated Sciences for Life, Hiroshima University, Higashi-Hiroshima 739-0046, Japan. ✉email: ktanimo@hiroshima-u.ac.jp

Figure 1. Effects of CSE on *ACE2* expression in human cell lines. **(a,b)** Expression levels of *CYP1A1* and *ACE2* genes in various concentrations of CSE treated HepG2 (Liver origin) cells for 24 h were evaluated by qRT-PCR. Relative gene expression levels were calculated by using *ACTB* expression as the denominator for each cell line ($n = 3$). For all quantitative values, the average and SD are shown. Statistical significance was calculated for the indicated paired samples with ** representing $P < 0.01$. Gene set enrichment analyses for gene lists analyzed by RNA-seq were performed with Metascape. Upregulated genes [$\log_2(\text{CSE-DMSO}) \geq 1$] **(c)** in CSE treated HepG2 cells and downregulated genes [$\log_2(\text{CSE-DMSO}) \leq -1$] **(e)** were enriched by gene ontology (GO) term. Process enrichment analyses using TRRUST showed human transcriptional regulatory interactions in upregulated genes **(d)**. AHR and ARNT, hetero-dimeric transcriptional partners, are indicated with red boxes.

compounds, such as 2,3,7,8-tetrachlorodibenzo-*p*-dioxin (TCDD), 3,3',4,4',5-pentachlorobiphenyl-126 (PCB126), 6-formylindolo(3,2-*b*)carbazole (FICZ), and omeprazole (OMP), and their physiological and pathological significance, especially in regard to the immune system, have received much attention^{15–19}.

In this study, we therefore aimed to clarify the effects of AHR agonists on *ACE2* expression in mammalian cells to better understand the role of *ACE2* in the SARS-CoV-2 internalization mechanism.

Results

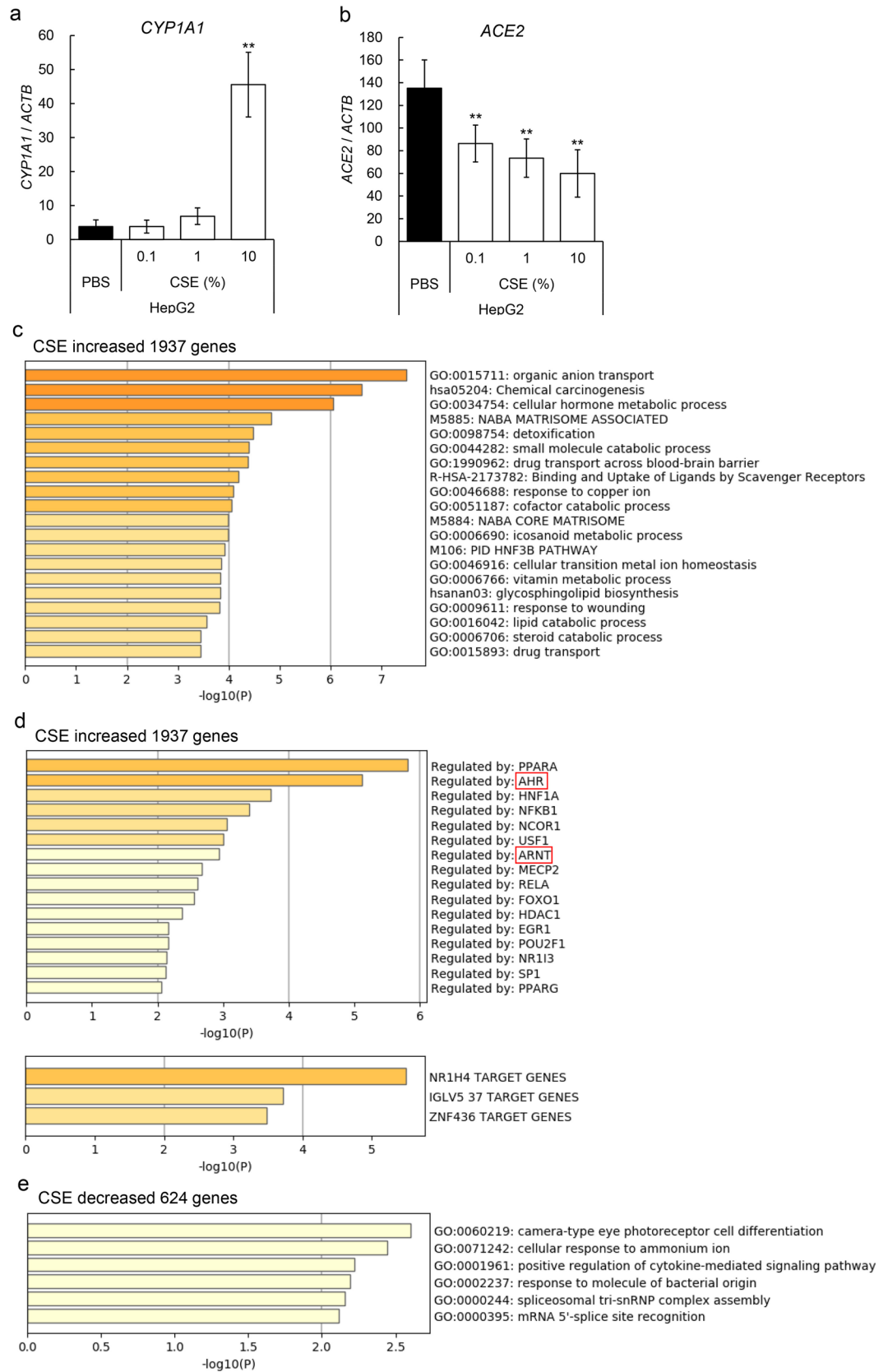
Effects of cigarette smoke extract (CSE) on *ACE2* expression in human cell lines. At first we examined expression levels of the SARS-CoV-2 viral receptor *ACE2* in various cell lines by using quantitative RT-PCR (qRT-PCR) (see Supplementary Fig. S1a online). Results demonstrated that *ACE2* expression level varied among the cell lines, and HSC2 (oral cavity origin), PC9 (lung origin), and HepG2 (liver origin), which had the highest levels of *ACE2* expression, were used in the first experiment. The cells were treated with various doses of cigarette smoke extract (CSE) for 24 h, after which expression level of cytochrome P450 family 1 subfamily A member 1 (*CYP1A1*) gene, which is known to be CSE-inducible, was evaluated with qRT-PCR. As expected, CSE treatment induced expression of *CYP1A1* in HepG2 cells in a dose-dependent manner (Fig. 1a). CSE treatment also induced expression of *CYP1A1* in PC9 cells, but expression was only slightly increased in HSC2 cells (Supplementary Fig. S1b). Interestingly, *ACE2* expression was significantly reduced in CSE-treated HepG2 cells in a dose-dependent manner, and was slightly reduced in PC9 and HSC2 cells (Fig. 1b and Supplementary Fig. S1c).

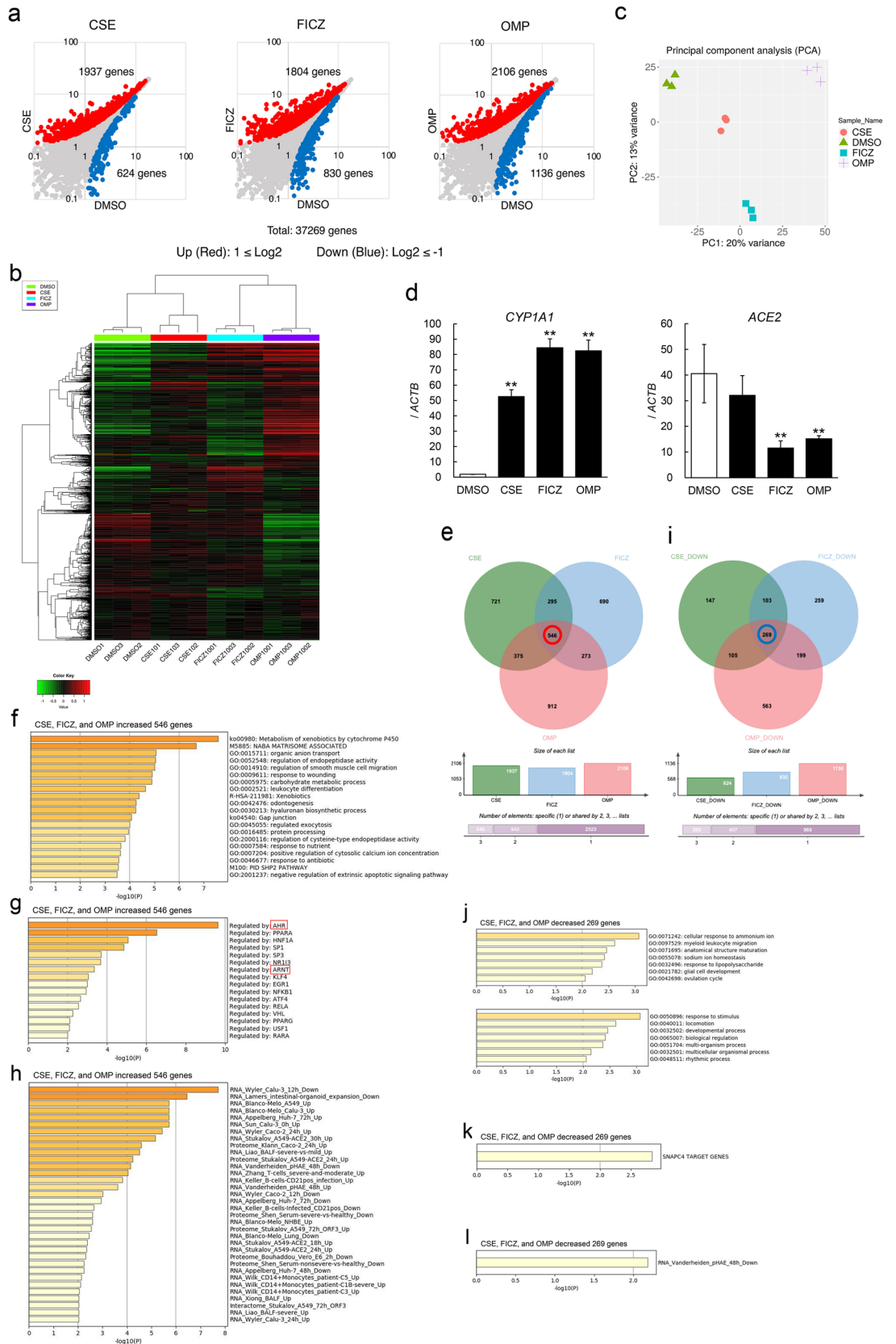
RNA-seq analysis of CSE treated HepG2 cells. To elucidate cellular responses to treatment with CSE, comprehensive gene expression was investigated with RNA-seq analysis. Results demonstrated that CSE increased the expression of 1937 genes and decreased that of 624 genes in HepG2 cells. Gene set enrichment analysis demonstrated that CSE increased the expressions of genes related to a variety of intracellular signals, such as organic anion transport, chemical carcinogenesis, and cellular hormone metabolic processes, which were regulated by various transcription factors, including PPAR, AHR, HNF1A, ARNT, and GATA4 (Fig. 1c,d). CSE-decreased genes indicated the involvement of signals, such as camera-type eye photoreceptor cell differentiation, cellular response to ammonium ion, and positive regulation of cytokine-mediated signaling pathway, although they were not significant (Fig. 1e). Among them, we first focused on AHR signals, which were executed by heterodimeric transcription factors of AHR and ARNT.

RNA-seq analysis of HepG2 cells treated with AHR agonists. To more directly observe the mechanism by which AHR signal acts on *ACE2* expression, effects of AHR agonists, such as FICZ and OMP, were evaluated in HepG2 cells. RNA-seq analysis demonstrated that FICZ and OMP increased expression of 1804 or 2106 genes, respectively, and decreased that of 830 or 1136 genes, respectively (Fig. 2a). Hierarchical clustering and principal component analysis (PCA) indicated that signals regulated by FICZ and OMP were relatively more similar than they were with those regulated by CSE, but the transcriptome of FICZ differed from that of OMP, as judged from the PCA result (Fig. 2b,c). The RNA-seq data suggested that the *CYP1A1* gene was strongly induced in HepG2 cells with FICZ and OMP treatments, but expression of the *ACE2* gene was clearly inhibited (Fig. 2d). A Venn diagram indicated that 546 genes were commonly upregulated and 269 genes were commonly downregulated in CSE-, FICZ-, or OMP-treated cells (Fig. 2e,i). Gene set enrichment analysis demonstrated that commonly regulated genes were related to metabolism of xenobiotics by cytochrome P450, which is known to be regulated by an AHR signal (Fig. 2f,g,j,k). Interestingly, an RNA-seq dataset composed of SARS-CoV-2 infection experiments (Coronascape: a customized version of Metascape bioinformatic platform that provides a central clearinghouse for scientists to laser focus their OMICS analysis and data-mining efforts) suggested that the commonly regulated genes noted here overlapped with the genes modified after SARS-CoV-2 infection (Fig. 2h,l).

Effects of AHR agonists on *ACE2* expression in HepG2 cells. qRT-PCR analysis demonstrated that FICZ and OMP efficiently induced expression of the AHR-target gene, *CYP1A1*, in a dose-dependent manner (Fig. 3a). Importantly, treatment with FICZ or OMP significantly suppressed *ACE2* expression in HepG2 cells (Fig. 3b). Furthermore, immunoblotting analysis confirmed that *ACE2* protein expression was suppressed by treatment with FICZ or OMP, consistent with their effect on *ACE2* gene expression (Fig. 3c). Analysis of the dose dependence of FICZ and OMP demonstrated that induction of *CYP1A1* and suppression of *ACE2* by FICZ both appeared to saturate at approximately 40 nM, whereas corresponding effects of OMP increased up to 100 μM (Fig. 3d–g).

Next, time-dependency of AHR agonists was evaluated. Treatment with 100 nM of FICZ increased *CYP1A1* expression to a maximum at 24 h, after which it decreased up to 72 h, whereas *ACE2* expression was suppressed





◀ **Figure 2.** Comprehensive RNA-seq gene expression analyses of HepG2 cells treated with AHR agonists. (a) Scatter plots of gene expressions (read counts) analyzed by RNA-seq in CSE (left), FICZ (middle), and OMP (right) treated HepG2 cells are shown. Upregulated genes [$\log_2(\text{CSE, FICZ, or OMP-DMSO}) \geq 1$] and downregulated genes [$\log_2(\text{CSE, FICZ, or OMP-DMSO}) \leq -1$] are indicated as red and blue dots. Hierarchical clustering (b) and principal component analysis (PCA) (c) for results of RNA-seq were performed with iDEP 0.91. (d) Gene expression levels of *CYP1A1* (left) and *ACE2* (right) genes in HepG2 analyzed with RNA-seq were validated with quantitative RT-PCR. Venn diagrams of genes upregulated (e) and downregulated (i) with CSE, FICZ, or OMP treatment in HepG2 cells are shown. Upregulated (f,g) and downregulated (j,k) genes commonly regulated were enriched by GO term and TRRUST. AHR and ARNT are indicated with red boxes. Enrichment analyses of upregulated (h) and downregulated (l) genes were also performed with Coronascope (coronascope.org), a one-stop meta-analysis resource of large-scale omics data.

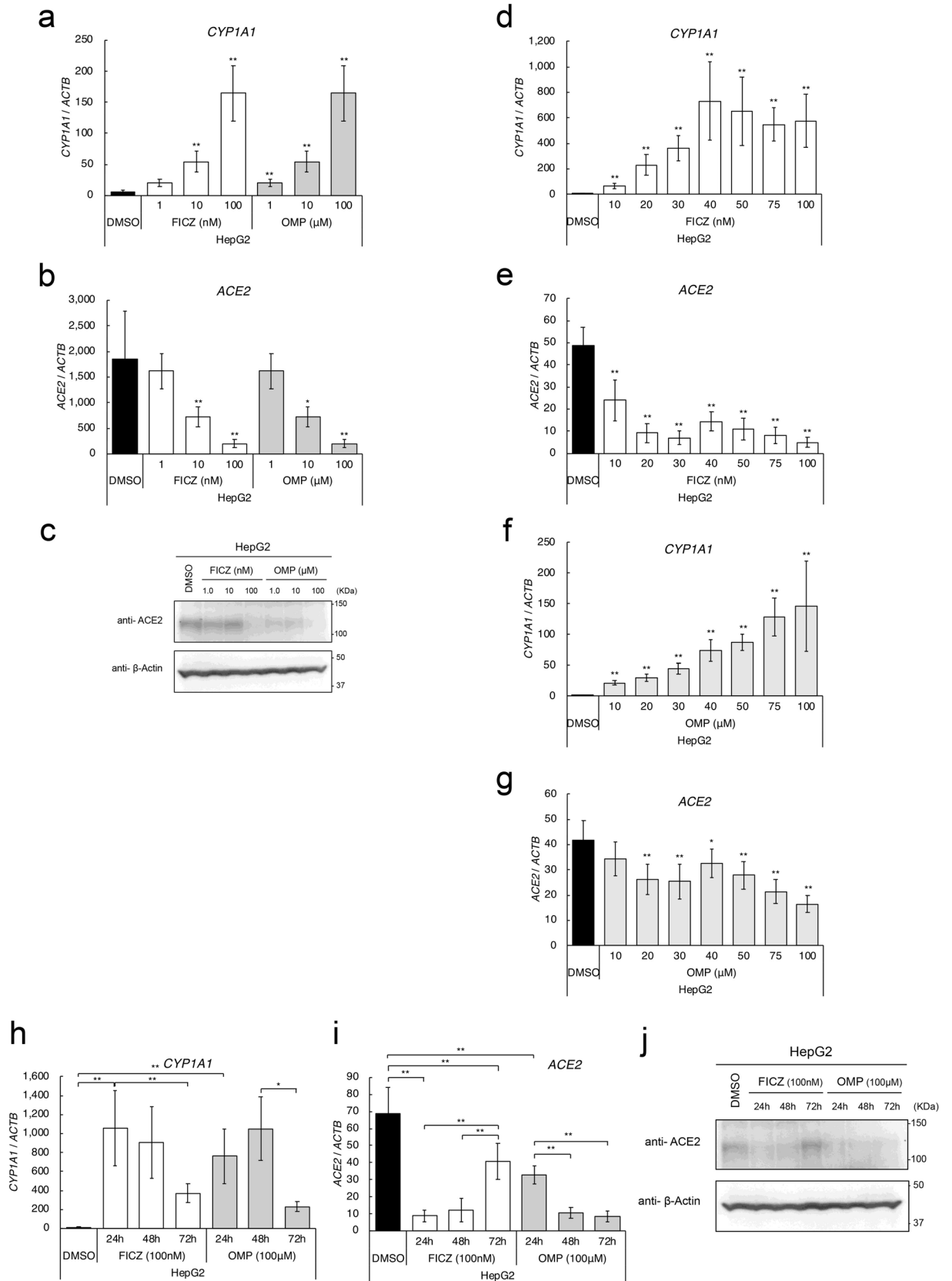
to the greatest extent at 24 h followed by a return to the original expression level at 72 h (Fig. 3h,i). Treatment with 100 μM OMP produced delayed responses in comparison with FICZ, the highest *CYP1A1* induction and greatest *ACE2* suppression being at 48 h (Fig. 3h,i). These observations were also confirmed by protein levels with immunoblotting analysis (Fig. 3j).

Role of AHR in *ACE2* suppression in HepG2 cells. To confirm that the effects of FICZ and OMP on *ACE2* suppression were actually dependent on AHR, knock-down experiments were performed. Effective knock-down of *AHR* in DMSO or FICZ treated HepG2 cells was confirmed with qRT-PCR, and *CYP1A1* induction with FICZ treatment was significantly inhibited in AHR knocked-down cells (Fig. 4a,b). Under this condition, *ACE2* expression in AHR knocked-down cells after treatment with FICZ increased up to the level in control cells, indicating a critical role of AHR in FICZ-induced *ACE2* suppression (Fig. 4c).

Effects of AHR agonists on SARS-CoV-2 infection of Vero E6 cells. To clarify the effect of AHR agonist-induced *ACE2* suppression on SARS-CoV-2 infection of mammalian cells, Vero E6 cells expressing *TMPRSS2*, which are known to be susceptible to SARS-CoV-2 infection, were employed in infection experiments²⁰. *ACE2* expression in Vero E6 cells was first evaluated by qRT-PCR and found to be downregulated by treatment with FICZ or OMP (Fig. 5a). Immunoblotting analysis with antibody against a specific SARS-CoV-2 protein, nucleocapsid protein, demonstrated that pre-treatment with FICZ or OMP decreased levels of nucleocapsid protein in a dose-dependent manner, suggesting a decrease in the number of viruses infecting the cells (Fig. 5b).

Discussion

ACE2 was identified as the virus receptor during the first SARS-CoV epidemic^{21–24}. SARS-CoV-2 spike protein (S-protein) has been shown to bind *ACE2* on host cells; the S-protein undergoes a proteolytic cleavage between the S1 and S2 subunits by the type II transmembrane serine protease (*TMPRSS2*), resulting in receptor-mediated internalization of the virus. Alternatively, other less important pathways may involve cathepsin L, an endo-lysosomal host cell protease, and furin protease whose target-cleavage sites are suggested to exist in SARS-CoV-2 S-protein but not in SARS-CoV^{21–24}. Therefore, modulators of expression levels of related proteins, especially *ACE2*, may regulate the process of SARS-CoV-2 infection. We here demonstrated that CSE, FICZ, and OMP, which could all act as agonists of AHR, suppressed the expression of *ACE2* in mammalian cells, resulting in suppression of internalization of SARS-CoV-2. *ACE2* expression was significantly decreased in CSE-treated HepG2 cells, whereas *CYP1A1* expression was induced. *ACE2* expression was slightly decreased in PC9 and HSC2 cells, in which *CYP1A1* expression was slightly increased. These results suggest that *ACE2* reduction is inversely correlated with induction of one of the well-known AHR target genes, *CYP1A1*, although treatment optimization is necessary in each cell line. RNA-seq analysis of CSE treated HepG2 cells also demonstrated that CSE treatment modified a variety of intracellular signals that are regulated by the transcription factors PPAR, AHR, HNF1A, and GATA4 (Fig. 1c–e). Furthermore, treatment with FICZ or OMP modified many important signals, such as response to wounding, metabolism of xenobiotics by cytochrome P450, the matrisome, and leukocyte differentiation, which were strongly suggested to be regulated by AHR (Supplementary Fig. S2). As expected, treatment with FICZ (a tryptophan metabolite) or OMP (a proton pump inhibitor) effectively induced *CYP1A1* expression in HepG2 cells in a dose-dependent manner. In addition, both AHR agonists clearly reduced *ACE2* expression at both the mRNA and protein levels. RNA-seq interestingly indicated that OMP seemed also to modify expression of *TMPRSS2* among SARS-CoV-2 internalization-related proteins, but CSE and FICZ did not, suggesting that OMP may be able to suppress SARS-CoV-2 infection more effectively (Supplementary Fig. S2i). Importantly, knock-down experiments of *AHR* confirmed that reduction of *ACE2* with FICZ treatment was dependent on AHR, although details of the molecular mechanism are as yet undetermined. There are several reports of AHR-mediated suppression of gene expression. One is that AHR suppresses thymic stromal lymphopoietin (*TSLP*) gene expression via phosphorylation of p300 by Protein Kinase C (PKC) δ , resulting in decreases in acetylation and DNA binding activity of NF- κ B²⁵. Another is decreased expression of the AP-1 family member *Junb*, which was substantially upregulated in the inflamed skin of *Ahr*-deficient mice²⁶. Finally, AHR was further demonstrated to form a complex with Stat1 and NF- κ B in macrophages stimulated by lipopolysaccharide (LPS), resulting in inhibition of promoter activity of the *IL6* gene²⁷. Since Genome Browser notes that ChIP-seq datasets in ENCODE actually indicate p300 and JUN binding on the human *ACE2* gene, *ACE2* downregulation by AHR agonist treatments might occur via functional interactions between AHR and those transcription factors. Furthermore, RNA-seq analysis in the present study revealed that treatment with several AHR agonists



◀**Figure 3.** Effects of AHR agonists on *ACE2* expression in HepG2 cells. Expression levels of *CYP1A1* (a), and *ACE2* (b) genes in various concentrations of FICZ or OMP treated HepG2 cells were evaluated by quantitative RT-PCR. (c) Protein expression levels of *ACE2* in various concentrations of FICZ or OMP treated HepG2 cells were evaluated by immunoblotting analysis (n = 3). A representative result is shown. Dose-dependent regulation of *CYP1A1* (d,f) and *ACE2* (e,g) gene expressions with FICZ or OMP treatments were evaluated by quantitative RT-PCR. Time-dependent regulation of *CYP1A1* (h) and *ACE2* (i) gene expressions with 100 nM of FICZ or 100 μM of OMP treatments were evaluated by quantitative RT-PCR. (j) Protein expression levels of *ACE2* were evaluated by immunoblotting analysis (n = 3). Relative gene expression levels were calculated by using *ACTB* expression as the denominator for each cell line (n = 3). For all quantitative values, the average and SD are shown. Statistical significance was calculated for the indicated paired samples with * representing $P < 0.05$ and ** $P < 0.01$.

downregulated some GATA4-regulated genes in HepG2 cells, so crosstalk between AHR and GATA4 might also be a possible mechanism of *ACE2* regulation (Supplementary Fig. S2g).

Another interesting observation in this study was the difference in time course effects of FICZ and OMP. FICZ seemed to affect *ACE2* expression early and suppression by FICZ was quickly reduced, but the effect of OMP seemed to be more gradual and suppression by OMP remained up to 72 h. This may be because of different activities and kinetics of their metabolism. Several other tryptophan metabolites, indole 3-carbinol (I3C), indoleacetic acid (IAA), tryptamine (TA), and L-kynurenine (KYN), and proton pump inhibitors, rabeprazole sodium (RBP), lansoprazole (LSP), and tenatoprazole (TNP), were also tested as to whether they regulate *ACE2* expression; it was demonstrated that most of them decreased expression of *ACE2* with a variety of actions and increased expression of *CYP1A1* (Supplementary Fig S3a,b). Similar differences were also observed among cell lines tested here (Fig. 1 and Supplementary Fig S1). Optimization of each compound will be necessary in the next steps (in vivo experiments and clinical studies), although most of the tryptophan metabolites and proton pump inhibitors other than CSE seem to be safely applicable to clinical therapeutic research. Furthermore, inhibitory effects of those compounds on infections with SARS-CoV-2 variants would be interesting to test, since many mutations in the virus have been reported so far²⁸. On the other hand, one limitation of this strategy might be that these drugs do not target the SARS-CoV-2 virus itself but just modify cellular susceptibility to it. Combination therapies of AHR agonists with anti-virus drugs, such as favipiravir or remdesivir, are therefore possible strategies for clinical application.

In addition to modifying cellular susceptibility to SARS-CoV-2, treatment with AHR agonists might stimulate immune response in the treated cells without virus infection. An RNA-seq dataset composed of SARS-CoV-2 infection experiments suggested that genes regulated by CSE, FICZ, and OMP overlapped with genes modified by SARS-CoV-2 infection, suggesting that stimulation of the immune system is involved (Fig. 2h,i, and Supplementary Fig. S2d,h). These observations might signify a potentially useful clinical application, although further investigation will be necessary to elucidate the details.

In conclusion, we here demonstrated that treatment with AHR agonists decreased expression of *ACE2* in mammalian cells, resulting in suppression of SARS-CoV-2 infection (Fig. 6). Application of these compounds in clinical research and in clinical practice might be warranted.

Materials and methods

Chemicals. All chemicals were analytical grade and were purchased from FUJIFILM Wako Pure Chemicals, Sigma-Aldrich, or Tokyo Chemical Industry (TCI).

CSE preparation. CSE was prepared by using a modified method reported previously²⁹. A detailed protocol is available at protocols.io (<https://dx.doi.org/10.17504/protocols.io.bnymmfu6>). Briefly, 5 filtered cigarettes were smoked consecutively through an experimental apparatus with a constant airflow (0.3 L/min) driven by a syringe, and the smoke was bubbled through 10 mL of phosphate buffered saline (PBS). The CSE obtained was then passed through a 0.22-μm filter (Millipore). The CSE was prepared immediately before each experiment.

Cell lines and RNA preparation. Human and monkey cell lines were purchased from the Japanese Cancer Research Resource Bank (JCRRB) and have been maintained as original stocks. The cells were normally maintained in RPMI1640 or DMEM (NACALAI TESQUE) containing 10% fetal bovine serum (FBS; BioWhittaker) and 100 μg/mL kanamycin (Sigma-Aldrich), and were used within 6 months of passage from original stocks. For this study, cells (1×10^6) were seeded on 10 cm diameter dishes and incubated for 24 h, then treated with various kinds of chemicals for the indicated periods. They were then harvested for expression analysis with RNA-seq, quantitative RT-PCR, and immunoblotting. For knock-down experiments, non-specific (siNS, No. 1027310) or *AHR* (siAHR, SI02780148) siRNA (QIAGEN, Inc.) was transfected with Lipofectamine™ RNAiMAX (Thermo Fisher Scientific Inc.) into HepG2 cells (1×10^6 /10 cm diameter dish) for 12 h, and then the cells were incubated with DMSO or FICZ for 24 h. Cells were then harvested and stored at -80°C until use. Total RNA was prepared from frozen cell pellets by using NucleoSpin® RNA (MACHEREY-NAGEL) according to the manufacturer's instructions.

Quantitative reverse transcription-polymerase chain reaction (RT-PCR). Two μg of total RNA extracted from each cell line was reverse-transcribed using a High-Capacity cDNA Archive™ Kit (Applied Biosystems). A two-hundredth aliquot of the cDNA was subjected to qRT-PCR with primers (final concentration 200 nM each) and MGB probe (final concentration 100 nM; the Universal Probe Library [UPL], Roche Diag-

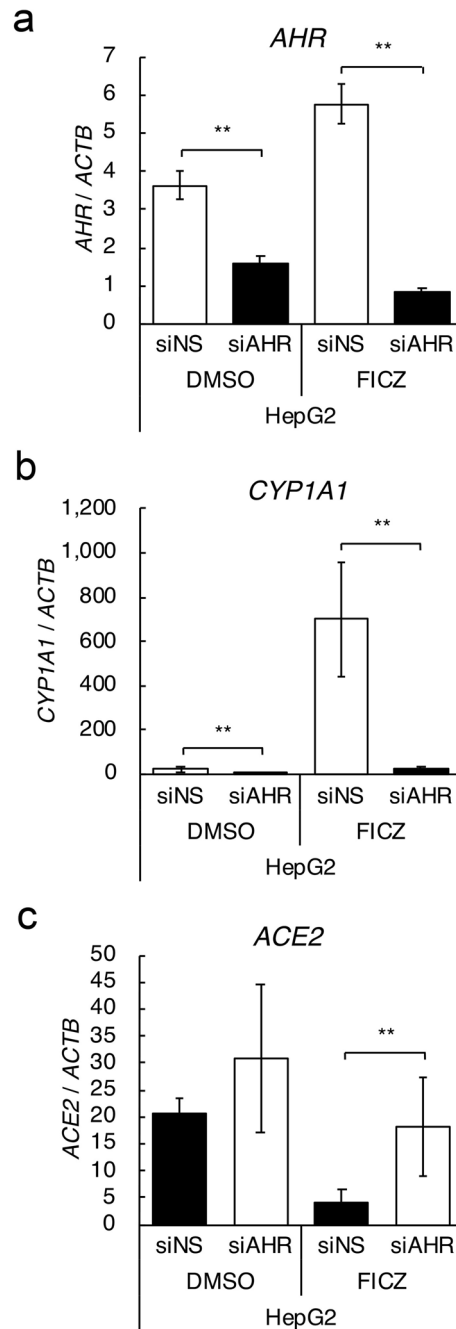


Figure 4. Roles of AHR on *ACE2* expression in HepG2 cells. Knock-down experiments were performed with specific siRNA for AHR. Expression levels of *AHR* (a), *CYP1A1* (b), and *ACE2* (c) genes in 100 nM of FICZ treated HepG2 cells were evaluated by quantitative RT-PCR. Relative gene expression level was calculated by using *ACTB* expression as the denominator for each cell line (n = 3). For all quantitative values, the average and SD are shown. Statistical significance was calculated for the indicated paired samples with ** representing $P < 0.01$.

nostics) sets as shown in Supplementary Table 1S for human *ACE2*, *CYP1A1*, *AHR*, and for primate *ACE2* and *ACTB*. Pre-Developed TaqMan™ Assay Reagents (Applied Biosystems) were used for human *ACTB* as an internal control. PCR reactions were carried out with a 7500 Real-Time PCR System (Applied Biosystems) under standard conditions. Relative gene expression levels were standardized by using a pooled cDNA derived from 17 various cancer cell lines, and were calculated by using *ACTB* expression as the denominator for each cell line.

RNA-sequence analysis. Total RNA was processed with a TruSeq Stranded mRNA sample prep kit (Illumina, San Diego, CA, USA)²⁹. Poly(A) RNA libraries were then constructed using the TruSeq Stranded mRNA

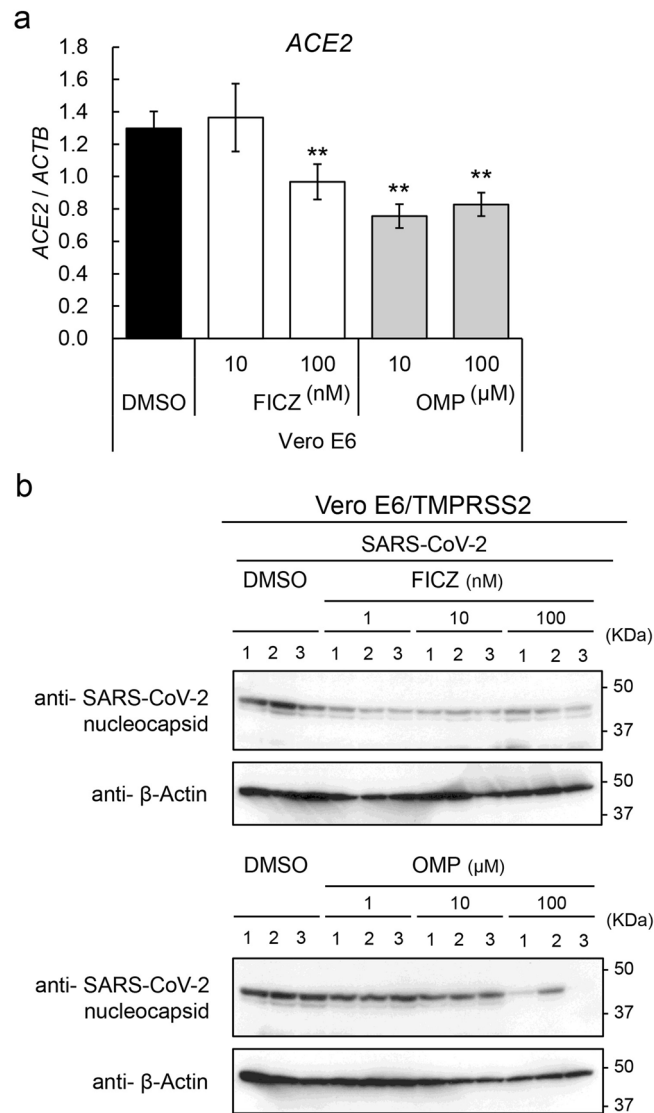


Figure 5. Effects of AHR agonists on SARS-CoV-2 infection to Vero E6 cells. **(a)** Expression level of *ACE2* gene in FICZ or OMP treated TMPRSS2 transfected Vero E6 cells was evaluated by quantitative RT-PCR. Relative gene expression level was calculated by using *ACTB* expression as the denominator for each cell line ($n = 3$). For all quantitative values, the average and SD are shown. Statistical significance was calculated for the indicated paired samples with ** representing $P < 0.01$. **(b)** Intracellular amount of nucleocapsid protein of SARS-CoV-2 was evaluated with immunoblotting analysis ($n = 3$). A representative result is shown.

library preparation kit (Illumina) and sequenced in 100-bp paired-end reads on an Illumina NovaSeq6000 platform³⁰. RNA-Seq was performed in triplicate.

RNA-seq reads were quantified by using *ikra* (v.1.2.2)³¹, an RNA-seq pipeline centered on Salmon³². The *ikra* pipeline automated the RNA-seq data-analysis process, including the quality control of reads [sra-tools v.2.10.7, Trim Galore v.0.6.3³³ using Cutadapt v.1.9.1³⁴], and transcript quantification (Salmon v.0.14.0, using reference transcript sets in GENCODE release 31 for humans, and tximport v.1.6.0). These tools were used with default parameters. Count tables were imported into integrated differential expression and pathway analysis (iDEP v.0.91), an integrated web application for gene ontology (GO) analysis of RNA-seq data (<http://bioinformatics.sdstate.edu/idep/>)³⁵. Quantified transcript reads were filtered at a threshold of 0.5 counts per million (CPM) in at least one sample and transformed as $\log_2(\text{CPM} + c)$ with EdgeR (3.28.0), with a pseudocount c value of 4. Gene set enrichment analysis was performed in iDEP with the fold-change values returned by DESeq2 (1.26.0). False positive rates of $q < 0.05$ were considered enriched and investigated further with Metascape³⁶. The TRRUST method^{37,38}, which analyzes human transcriptional regulatory interactions, was applied by using the web-based Metascape, a gene annotation and analysis resource algorithm (<https://metascape.org/>)³⁶. A Venn diagram was constructed by using *jvenn*, a plug-in for the jQuery javascript library (<http://jvenn.toulouse.inra.fr/app/index.html>).

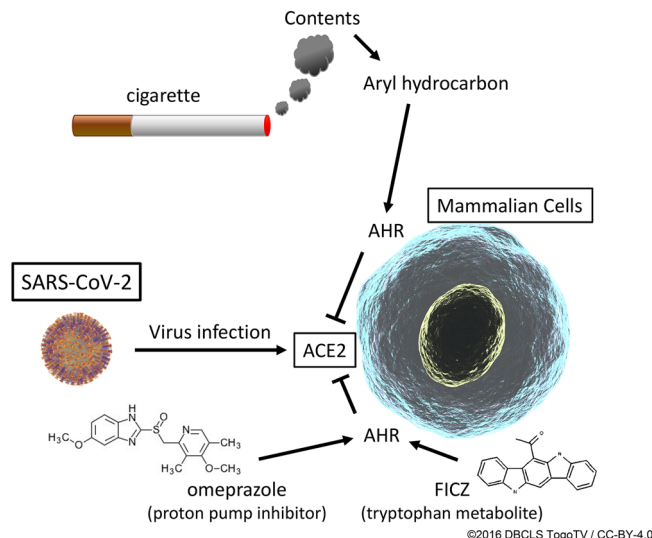


Figure 6. Schematic representation of effects of AHR agonists. CSE, FICZ, and OMP decreased expression of ACE2 via AHR activation, resulting in suppression of SARS-CoV-2 infection in mammalian cells. Illustrations of the virus and the cell have been reproduced from ©2016 DBCLS TogoTV/CC-BY-4.0 (<https://togotv.dbcls.jp/>).

Virus infection analysis. To observe the efficiency of infection of mammalian cells by SARS-CoV-2, SARS-CoV-2/Jp/Hiroshima-46059T/2020 and TMPRSS2 transfected Vero E6 cells were employed²⁰. Vero E6/TMPRSS2 cells in a 24 well plate were treated with FICZ or OMP for 24 h before virus infections. The cells were then infected with SARS-CoV-2 at an input multiplicity of infection of 0.01 and incubated for 24 h. After the cells were washed with PBS, cell lysates were obtained by directly adding SDS-sample buffer and then subjected to immunoblotting analysis.

Immunoblot analysis. To analyze protein expression, whole cell extracts were prepared from cultured cells with the indicated treatments as previously described³⁹. Fifty µg of extracts was blotted onto nitrocellulose filters following SDS-polyacrylamide gel electrophoresis. Anti-ACE2 (GTx101395, GeneTex), anti-SARS-CoV-2 nucleocapsid (GTx632269, GeneTex), or anti-β-actin (A5441, Sigma-Aldrich) was used as the primary antibody, diluted 1:1000, 1:1000, or 1:5000, respectively. A 1:2000 dilution of anti-mouse or anti-rabbit IgG horseradish peroxidase conjugate (#7076, #7074, Cell Signaling TECHNOLOGY) was used as a secondary antibody. Immunocomplexes were visualized by using the enhanced chemiluminescence reagent ECL Plus (Amersham Life Science).

Statistical analysis. Statistical tests were based on the ANOVA test, Student's *t* test, Dunnett's test, or the Games-Howell test in SPSS Statistics version 17.0 (IBM).

Data availability

Raw sequencing data were deposited in the DNA Data Bank of Japan Sequence Read Archive (<https://www.ddbj.nig.ac.jp/dra/index-e.html>; accession nos. DRR264900–DRR264911).

Received: 14 March 2021; Accepted: 5 August 2021

Published online: 17 August 2021

References

1. WHO. <https://www.who.int/emergencies/diseases/novel-coronavirus-2019>.
2. Vardavas, C. I. & Nikitara, K. COVID-19 and smoking: A systematic review of evidence. *Tob. Induc. Dis.* **18**, 20 (2020).
3. Berlin, I., Thomas, D., Le Faou, A. L. & Cornuz, J. COVID-19 and smoking. *Nicotine Tob. Res.* **22**, 1650–1652 (2020).
4. Guo, E. R. Active smoking is associated with severity of coronavirus disease 2019 (COVID-19): An update of meta-analysis. *Tob. Induc. Dis.* **18**, 37 (2020).
5. Kashyap, V. K. *et al.* Smoking and COVID-19: Adding fuel to the flame. *Int. J. Mol. Sci.* **21**, 6581 (2020).
6. Smith, J. C. *et al.* Cigarette smoke exposure and inflammatory signaling increase the expression of the SARS-CoV-2 receptor ACE2 in the respiratory tract. *Dev. Cell* **53**, 514–529 (2020).
7. Rentsch, C. T. *et al.* Covid-19 testing hospital admission, and intensive care among 2,026,227 United States Veterans aged 54–75 years. *medRxiv*. <https://doi.org/10.1101/2020.04.09.20059964> (2020).
8. Miyara, M. *et al.* Low rate of daily active tobacco smoking in patients with symptomatic COVID-19. *Qeios* <https://doi.org/10.32388/WPP19W.4> (2020).
9. de Lusignan, S. *et al.* Risk factors for SARS-CoV-2 among patients in the Oxford Royal College of General Practitioners Research and Surveillance Centre primary care network: A cross-sectional study. *Lancet Infect. Dis.* **20**, 1034–1042 (2020).
10. Williamson, E. J. *et al.* Factors associated with COVID-19-related death using OpenSAFELY. *Nature* **584**, 430–436 (2020).

11. Zhang, L. *et al.* Effects of cigarette smoke and its active components on ulcer formation and healing in the gastrointestinal mucosa. *Curr. Med. Chem.* **19**, 63–69 (2012).
12. AlQasrawi, D., Qasem, A. & Naser, S. A. Divergent effect of cigarette smoke on innate immunity in inflammatory bowel disease: A nicotine-infection interaction. *Int. J. Mol. Sci.* **21**, 5801 (2020).
13. Hankinson, O. The aryl hydrocarbon receptor complex. *Annu. Rev. Pharmacol. Toxicol.* **35**, 307–340 (1995).
14. Moorthy, B., Chu, C. & Carlin, D. J. Polycyclic aromatic hydrocarbons: from metabolism to lung cancer. *Toxicol. Sci.* **145**, 5–15 (2015).
15. Denison, M. S. & Nagy, S. R. Activation of the aryl hydrocarbon receptor by structurally diverse exogenous and endogenous chemicals. *Annu. Rev. Pharmacol. Toxicol.* **43**, 309–334 (2003).
16. Gutiérrez-Vázquez, C. & Quintana, F. J. Regulation of the immune response by the aryl hydrocarbon receptor. *Immunity* **48**, 19–33 (2018).
17. Rothhammer, V. & Quintana, F. J. The aryl hydrocarbon receptor: An environmental sensor integrating immune responses in health and disease. *Nat. Rev. Immunol.* **19**, 184–197 (2019).
18. Murray, I. A., Patterson, A. D. & Perdew, G. H. Aryl hydrocarbon receptor ligands in cancer: Friend and foe. *Nat. Rev. Cancer* **14**, 801–814 (2014).
19. Gao, J. *et al.* Impact of the gut microbiota on intestinal immunity mediated by tryptophan metabolism. *Front. Cell. Infect. Microbiol.* **8**, 13. <https://doi.org/10.3389/fcimb.2018.00013> (2018).
20. Matsuyama, S. *et al.* Enhanced isolation of SARS-CoV-2 by TMPRSS2-expressing cells. *Proc. Natl. Acad. Sci. U.S.A.* **117**, 7001–7003 (2020).
21. Scialo, F. *et al.* ACE2: The major cell entry receptor for SARS-CoV-2. *Lung* **198**, 867–877 (2020).
22. Ziepeto, D., Palmeira, J. D. F., Argañaraz, G. A. & Argañaraz, E. A. ACE2/ADAM17/TMPRSS2 interplay may be the main risk factor for COVID-19. *Front. Immunol.* **11**, 576745. <https://doi.org/10.3389/fimmu.2020.576745> (2020).
23. Wan, Y., Shang, J., Graham, R., Baric, R. S. & Li, F. Receptor recognition by the novel coronavirus from Wuhan: An analysis based on decade-long structural studies of SARS coronavirus. *J. Virol.* **94**, e00127–e220 (2020).
24. Zhou, P. *et al.* A pneumonia outbreak associated with a new coronavirus of probable bat origin. *Nature* **579**, 270–273 (2020).
25. Jeong, H., Shin, J. Y., Kim, M. J., Na, J. & Ju, B. G. Activation of aryl hydrocarbon receptor negatively regulates thymic stromal lymphopoietin gene expression via protein kinase C δ -p300-NF- κ B pathway in keratinocytes under inflammatory conditions. *J. Invest. Dermatol.* **139**, 1098–1109 (2019).
26. Di Meglio, P. *et al.* Activation of the aryl hydrocarbon receptor dampens the severity of inflammatory skin conditions. *Immunity* **40**, 989–1001 (2014).
27. Kimura, A. *et al.* Aryl hydrocarbon receptor in combination with Stat1 regulates LPS-induced inflammatory responses. *J. Exp. Med.* **206**, 2027–2035 (2009).
28. Boehm, E. *et al.* Novel SARS-CoV-2 variants: the pandemics within the pandemic. *Clin. Microbiol. Infect.* <https://doi.org/10.1016/j.cmi.2021.05.022> (2021).
29. Kida, N. *et al.* Cigarette smoke extract activates hypoxia-inducible factors in a reactive oxygen species-dependent manner in stroma cells from human endometrium. *Antioxidants* **10**, 48 (2021).
30. Sumi, C. *et al.* Cancerous phenotypes associated with hypoxia-inducible factors are not influenced by the volatile anesthetic isoflurane in renal cell carcinoma. *PLoS ONE* **14**, e0215072 (2019).
31. Hiraoka, Y. *et al.* Ikra: RNAseq pipeline centered on Salmon. Zenodo <https://doi.org/10.5281/ZENODO.3352573> (2019).
32. Patro, R., Duggal, G., Love, M. I., Irizarry, R. A. & Kingsford, C. Salmon provides fast and bias-aware quantification of transcript expression. *Nat. Methods* **14**, 417–419 (2017).
33. Krueger, F. *Trim Galore*. https://www.bioinformatics.babraham.ac.uk/projects/trim_galore/ (accessed Oct 14, 2020).
34. Martin, M. Cutadapt removes adapter sequences from high-throughput sequencing reads. *EMBnet J.* **17**, 10–12 (2011).
35. Ge, S. X., Son, E. W. & Yao, R. iDEP: An integrated web application for differential expression and pathway analysis of RNA-Seq data. *BMC Bioinformatics* **19**, 534 (2018).
36. Zhou, Y. *et al.* Metascape provides a biologist-oriented resource for the analysis of systems-level datasets. *Nat. Commun.* **10**, 1523 (2019).
37. Han, H. *et al.* TRRUST v2: An expanded reference database of human and mouse transcriptional regulatory interactions. *Nucleic Acids Res.* **46**, D380–D386 (2018).
38. Han, H. *et al.* TRRUST: A reference database of human transcriptional regulatory interactions. *Sci. Rep.* **5**, 11432 (2015).
39. Tanimoto, K., Makino, Y., Pereira, T. & Poellinger, L. Mechanism of regulation of the hypoxia-inducible factor-1 alpha by the von Hippel-Lindau tumor suppressor protein. *EMBO J.* **19**, 4298–4309 (2000).

Acknowledgements

We greatly appreciate the technical support provided by Ms. Chiyo Oda. We also appreciate encouragement given by Dr. Shin-ichi Hayashi (Tohoku University) and Dr. Lorenz Poellinger (Karolinska Institutet). Illustrations of the virus and the cell in Figure 6 have been reproduced from ©2016 DBCLS TogoTV / CC-BY-4.0 (<https://togotv.dbcls.jp/>). This work was partly supported by the Program of the Network-type Joint Usage/Research Center for Radiation Disaster Medical Science, and JSPS KAKENHI Grant Number JP18K09768.

Author contributions

K.T. designed the study, performed experiments, analyzed data, wrote the initial draft and edited the manuscript, and took funding acquisition. K.H. and Y.M. analyzed data wrote the initial draft and edited the manuscript. T.F. analyzed data and edited the manuscript. T.N., N.T., and T.S. performed experiments and edited the manuscript. N.H. supervised the study. H.B. analyzed data and edited the manuscript.

Competing interests

The authors declare no competing interests.

Additional information

Supplementary Information The online version contains supplementary material available at <https://doi.org/10.1038/s41598-021-96109-w>.

Correspondence and requests for materials should be addressed to K.T.

Reprints and permissions information is available at www.nature.com/reprints.

Publisher's note Springer Nature remains neutral with regard to jurisdictional claims in published maps and institutional affiliations.



Open Access This article is licensed under a Creative Commons Attribution 4.0 International License, which permits use, sharing, adaptation, distribution and reproduction in any medium or format, as long as you give appropriate credit to the original author(s) and the source, provide a link to the Creative Commons licence, and indicate if changes were made. The images or other third party material in this article are included in the article's Creative Commons licence, unless indicated otherwise in a credit line to the material. If material is not included in the article's Creative Commons licence and your intended use is not permitted by statutory regulation or exceeds the permitted use, you will need to obtain permission directly from the copyright holder. To view a copy of this licence, visit <http://creativecommons.org/licenses/by/4.0/>.

© The Author(s) 2021